ISSN: 0975-8585

Research Journal of Pharmaceutical, Biological and Chemical Sciences

Removal of methylene blue and brilliant green dyes from aqueous solution by Ag_2O/MCM-41 nanoparticles.

S. A. El-Hakam*, Awad I. Ahmed, E. Abdel-Galil, Sh. M. EL-Dafrawy, and A. A. Al-Khamri

Chemistry Department, Faculty of science, Mansoura University, Mansoura, Egypt

ABSTRACT

Silver oxide (Ag_2O) nanoparticles loaded on MCM-41 mesoporous silica were synthesized by the impregnation-evaporation method. The structural characterization was investigated by transmission electron microscopy (TEM), X-ray diffraction (XRD) and Fourier transforms infrared (FTIR). The prepared materials were used for removal of methylene blue and brilliant green dyes from aqueous medium considering the effect of adsorbent dosage, pH, shaking time and initial dye concentration. The results showed that adsorption capacity of Ag_2O/MCM-41nanoadsorbent higher than pure MCM-41. The best results were obtained with 25% Ag_2O/MCM-41 which shows higher adsorption activity. The adsorption was found to follow the pseudo –second order adsorption kinetic model and fitted with Langmuir adsorption isotherm.

Keywords: Ag_2O nanoparticle, MCM-41, dyes, adsorption, kinetics

*Corresponding author

ISSN: 0975-8585

INTRODUCTION

Mesoporous silica (MCM-41) has a more significance impotence due to its large surface area, non-toxicity, high biocompatibility, inert framework and large pore volume [1].Therefore, it is used in many potential applications such as heterogeneous catalysis [2, 3], drug delivery [4-6], antibacterial applications [7], removal of pollutants from aqueous solutions [8], and photocatalytic activity [9]. The MCM-41 has a hexagonal shape with diameter from about 2 to 50nm. Pure-MCM-41 has a porous structure but with small activity due to inactive nature of silica. However, the metal or metal oxide modified MCM-41 mesoporous possesses large surface area, surface active sites and advanced adsorption capacity [10]. Classical methods for removal of dyes from aqueous solution involve adsorption on solid surface, oxidation, chemical coagulation, biological treatment, flotation and filtration. The adsorption is one of the most efficient isolation methods in removal of dyes and heavy metals, besides offering the possibility for regeneration, recovery, and recycling of the adsorbing materials [11-13]. The removal of dyes from aqueous solution is a very complex problem because of the extensive range of dyes properties and because of non-bio degradation nature of most dyes [14]. Adsorption has been found to be more excellent method for dyes removal compared with other methods because of its simple design, low operating cost and insensitivity to a toxic substance [15]. Activated carbon is extensively used as adsorbent due to its great adsorption capabilities for adsorption of large groups of organic compounds, but the cost of activated carbon is comparatively high and its regeneration is difficult, which limits its usage in dyes adsorption [16]. In recent decades, development of a modern adsorbent such as modified MCM-41, which has developed properties such as high adsorption capability, fast removal take attention from authors [17]. Brilliant green (BG) and Methylene blue (MB) dyes have been studied in many recent articles. MB or BG have been recommended as one of the most selected dyes due to many advantage, it can be readily obtained purely, easily adsorbed by most surfaces in the form ionic micelles of known aggregation number and chemically stable [18, 19].

In the present study, silver oxide nanoparticles embedded MCM-41 with different silver oxide nanoparticle ratio were produced and used as adsorbents for removal of methylene blue and brilliant green from water and different application conditions were considered including, effect of pH, shaking time, adsorbent dosage and initial dye concentration.

MATERIALS AND METHODS

Materials

Tetraethylorthosilicate (TEOS), NH_4OH, cetyltrimethylammoniumbromide (CTAB), silver nitrate, methylene blue and brilliant green were purchased from Alfa-Aeser and used without further purification.

Preparation of solid adsorbents:

Preparation of MCM-41:

MCM-41 was prepared according to the original method that proposed by Beck *et al*. [18]. 2.0 g cetyltrimethylammoniumbromide (CTAB) was added to 100 mL of distilled water with stirring until a clear solution, then we added 12.5 mL ammonium hydroxide solution (33 wt. %). The addition of ammonium hydroxide solution results in a sufficiently basic solution with a pH of about 13. After vigorous stirring for about 30 min, we added 10.0 mL of TEOS. A thick white solution is formed which generally necessitates manual stirring to ensure adequate gel homogeneity. The product filtered, washed with distilled water and dried at 120 ^{o}C. The products recovered was washed thoroughly with distilled water to ensure the removal of excess CTAB and ammonia. The result is a fluffy, white powder. Is dried overnight at 120 °C the mole product of the gel mixture was CTAB: TEOS: NH_4OH: H_2O = 0.22: 1.04: 1.39: 44.4 From the catalyst without being so harsh as to destroy the mesoporous silica skeleton. Samples are calcinated at 550 °C at the rate of 5 °C/ min. for six hours.

Preparation of Ag_2O/MCM-41:

Ag_2O nanoparticles was embedding into the pores MCM-41 nanocrystals by impregnation-evaporation method [20]. Suspension 0.5g MCM-41 in 100 mL distilled water then $AgNO_3$ was added to the suspension. The suspension of MCM-41-$AgNO_3$ was stirred in a water bath at 100 ºC till solvent was evaporated. The produced material was filtered and washed with distilled water, then dried at 100 ºC for 12 h and then heated for 2 h at 550 ºC.

ISSN: 0975-8585

Characterization

X-ray diffraction patterns was performed using PW 150 (Philips) using Ni-filtered Cu Kα radiation in the 2θ ranges of 1-10º (low angle) and 10º-80º (wide angle). FTIR spectra of prepared samples were scanned in KBr pellets, transmission spectra are measured in the range of 4000-400 cm^{-1}. TEM images were carried out using a Philips CM120 Biotwin electron microscope operating at 120 KV, the specimens were dispersed in isopropanol and dropped on a carbon-coated microgrid.

RESULTS AND DESICCATION

Characterization of solid adsorbents

X-ray diffraction patterns

Small angle XRD pattern of MCM-41 calcined at 550 °C is shown in Fig. 1. The well-defined XRD patterns were indexed based on three Bragg peaks, which were in hexagonal lattice system, characteristic of MCM-41 structure. The X-ray patterns of MCM-41 showed typically one to three reflections between 2θ = 2º to 5º. The reflection plane (100) at 2θ = 2.3º is due to the hexagonal array of parallel silicas tubes, while other two reflection planes (110) and (200) at 2θ = 4.0º and 4.8º due to the highly ordered arrangement of hexagonal arrays [21].

Fig. 2 represents samples containing 10, 25 wt. % Ag_2O calcined at 550 ºC and 25 wt. % Ag_2O calcined at 700 ºC. The XRD patterns of Ag_2O/MCM-41 demonstrate the typical Bragg reflection of the mesoporous MCM-41 material with a hexagonal array which is evidenced by the diffraction peaks at 2θ = 2.3º, 4.0º and 4.8º assignable to the (100), (110) and (200) silica planes, respectively [22]. This phenomenon shows that mesoporous building of MCM-41 is structurally unaffected after modification. In another word, the pore structure of MCM-41 was not destroyed during metal incorporation processes. The main difference between pure MCM-41 and Ag_2O/MCM-41 with different ratio of Ag_2O is the intensity of Ag_2O/MCM-41 diffraction peaks were decreased slightly with increasing the Ag_2O content because of pores filling of the host substance.

The wide-range XRD patterns were obtained by scanning the samples from 10° to 80° as presented in Fig. 3, which exhibits a number of peaks at 2θ = 37.4° (111), 44.1° (200), 63.9° (220) and 75.9° (311) where, the intensity of peaks are increased by the increase in the amount of Ag_2O content. The increase in Ag_2O ratio resulted in an increase in the degree of crystallization that can be noticed from the increasing of peak intensities (as shown in Fig. 3). Figure 4 shows the effect of calcination temperature on X-ray diffraction pattern for 25 wt. % Ag_2O/MCM-41. When the calcination temperature increases to 700 °C, the peak intensities are decreased, which may be due to the partially loss of Ag_2O loaded MCM-41 [22, 23].

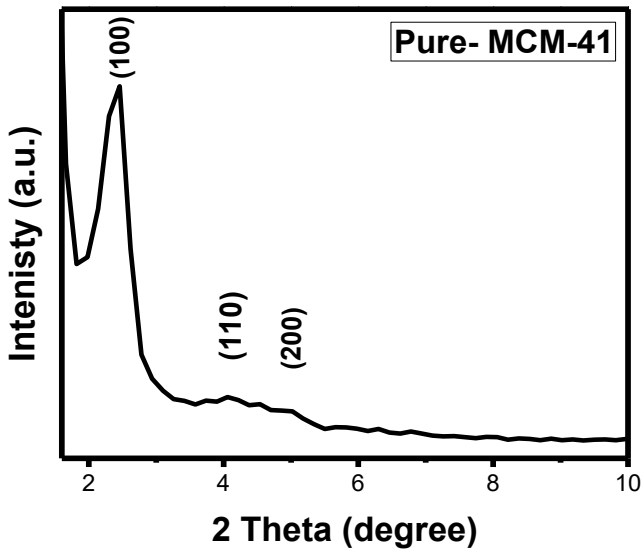

Fig. (1): small angle XRD patterns of Pure MCM-41.

ISSN: 0975-8585

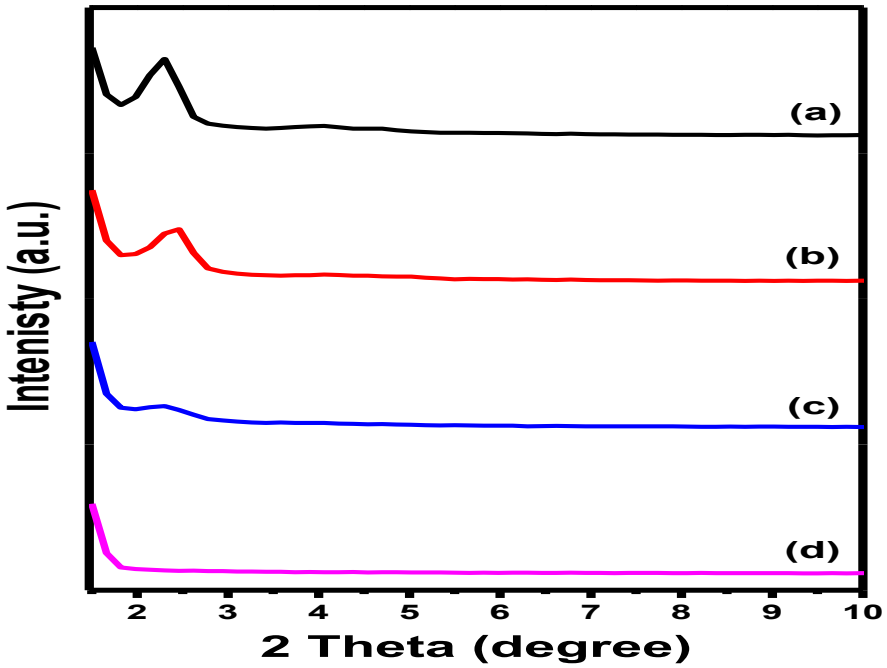

Fig. (2):small angle XRD pattern of (a) Pure MCM-41, (b), (c) 10, 25 wt. % Ag_2O/MCM-41(550ºC) (d) 25 wt. % Ag_2O/MCM-41(700ºC).

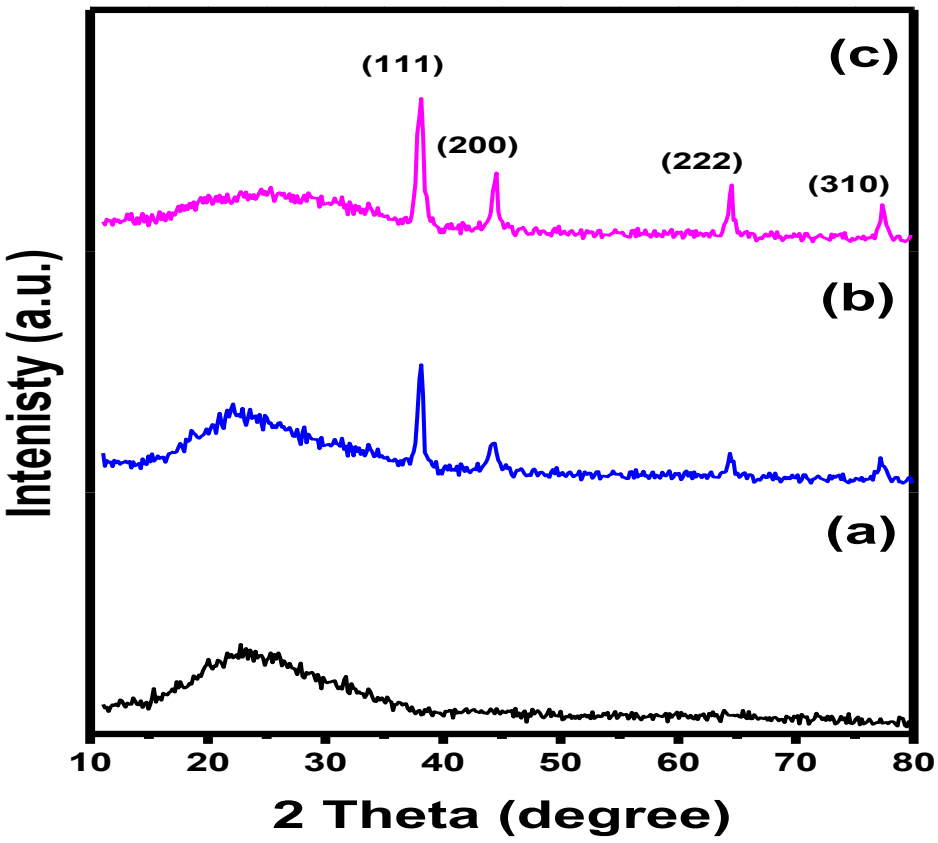

Fig. (3):Wide angle XRD pattern of (a) Pure-MCM-41 (b), (c) 10, 25 wt. % Ag_2O/MCM-41(550ºC).

ISSN: 0975-8585

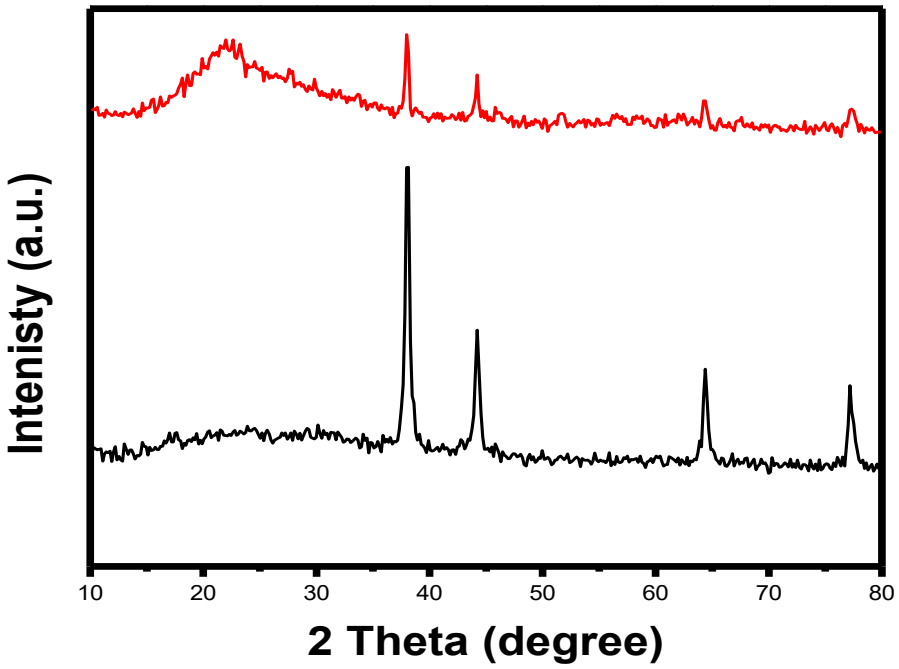

Fig. (4): High angle X-ray diffraction pattern of different calcination temperature (a) 25 wt. % Ag_2O/MCM-41(550ºC) and (b) 25 wt. % Ag_2O/MCM-41 (700ºC).

Transmission electron microscopy (TEM)

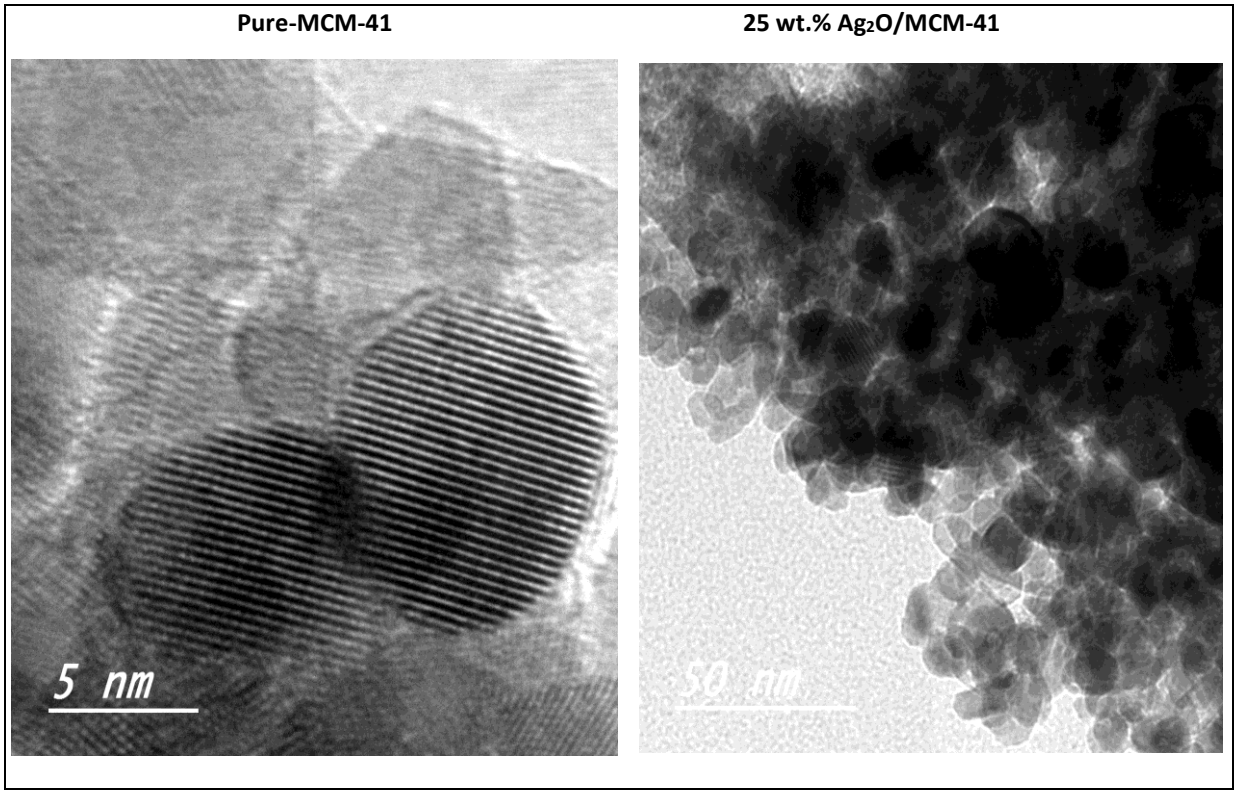

Fig. (5): TEM images of the pure-MCM-41 and 25 wt. % Ag_2O/MCM-41.

TEM images show that samples composed of amorphous silica, it shows an ordered structure with constant mesoporous arranges into hexagonal, honey comb-like lattice as shown in Fig. 5. The samples show regular pore size nearly 25 nm. TEM image of samples displays the existence of nanosized spherical particle and hexagonal array. The development of MCM-41 particles depends on the length of silicate rod-like micelles, which determined by the type of base used (ammonium hydroxide) which favour longer micelles, whereas, sodium hydroxide media favour shorter micelles [22, 24].

Fig. 5 displays TEM images of the morphology and microstructure of nanoadsorbent Ag_2O/MCM-41. The results show that irregular and similar sphere particles, with nanosize, nearly14-20 nm and the degree of crystallinity of the sample increased with content to 25 wt. % nano Ag_2O loaded on MCM-41. The number of black spots in the Figure (referred toAg_2O nanoparticles). The sample of 25 wt. % nanoadsorbent shows an enhanced crystallinity with the crystallite size ranging from 13-25 nm, which is in accordance with the results of X-ray diffraction [21].

Fourier transforms infrared Spectroscopy (FTIR).

Fig. 6 shows the spectra of pure MCM-41, 4, 10, 17, 25 and 35 wt % Ag_2O/MCM-41 samples calcinated at 550 ^oC in the region of 4000- 400 cm^{-1}. Absorption peaks at 1635 and 3463 cm^{-1} attributed to bending and stretching vibrations of the adsorbed water molecules, respectively. The strong vibration band at 1080 cm^{-1} in pure MCM-41 assigned to asymmetric stretching of Si-O-Si and shifted to 1089 cm^{-1} in case of Ag_2O/MCM-41 due to incorporation of Ag_2O in MCM-41 pores. The Si-O-Si from MCM-41 is observed at 1080- 1250 cm^{-1}, while the band at 802 and 1089 cm^{-1} in case of Ag_2O/MCM-41 samples attributed to symmetric and asymmetric stretching vibration of the Si-O bond, respectively. The band at 464 cm^{-1} indicates the bending vibration of Si-O-Si, and band at 960 cm^{-1} is due to the Si-O-Ag stretching vibration polarized or free vibration of the Si-OH band. The band at 960 cm^{-1} in Ag_2O/MCM-41 samples is high intense as compared to the peak in pure MCM-41. The peaks at 805 cm^{-1} in Ag_2O/MCM-41 samples is more broad and intense. The peak at 960 cm^{-1} in Ag_2O/MCM-41 is more intense and due to the Si-O-H vibration compared to MCM-41. This indicates that nanoAg_2O is bonded to silica by Si-O-Ag bond [22, 25-27].

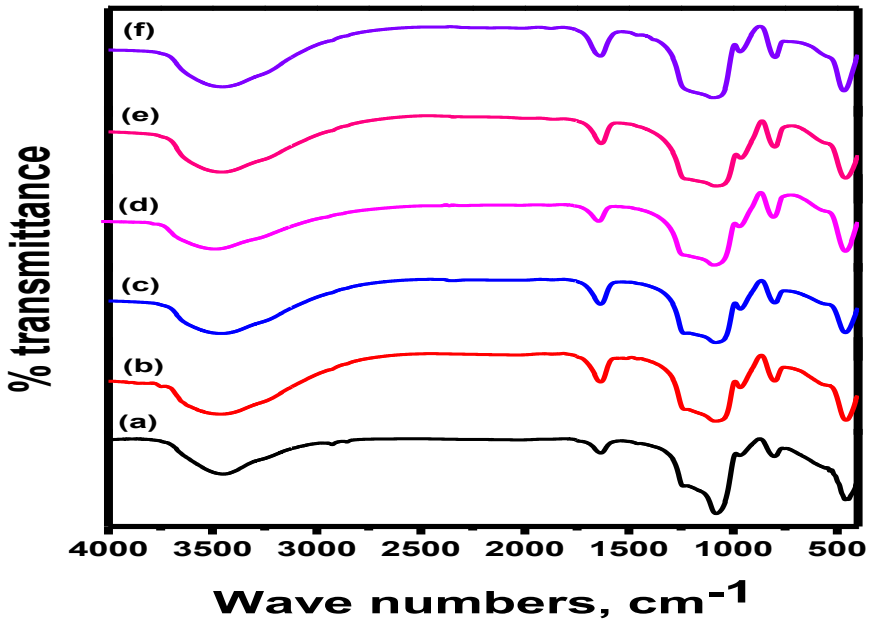

Fig. (6): FTIR spectra of (a) pure MCM-41 (b) 4%, (c) 10%, (d) 17%, (e) 25% and (f) 35 wt. % Ag_2O loaded on MCM-41.

Fig. 7 displays the effect of calcination temperature on the FTIR spectra of 25% Ag_2O/MCM-41. When the calcination temperature increases to 700 ^oC, the intensities of the bands at 3454 and 1636 cm^{-1} are decreased while the shoulder at 960 cm^{-1} is disappeared, this is may be due to the loss part of Ag_2O loaded on MCM-41.

ISSN: 0975-8585

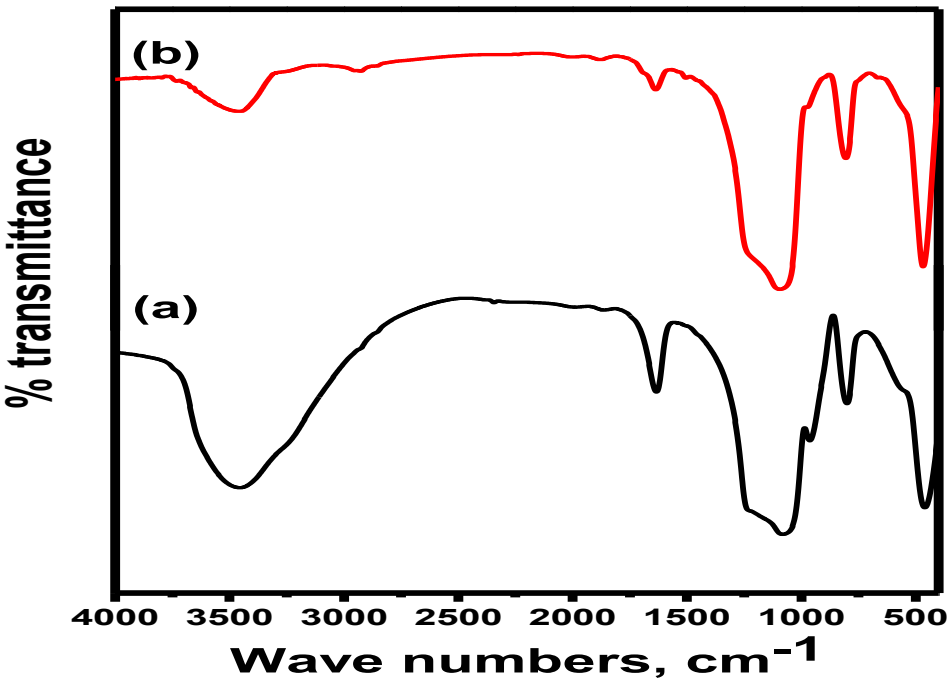

Fig. (7): FTIR spectra of 25 wt. % Ag_2O/MCM-41 calcined at (a) 550°C and (b) 700°C

Adsorption of methylene blue and brilliant green dyes

Effect of pH on the adsorption of dyes

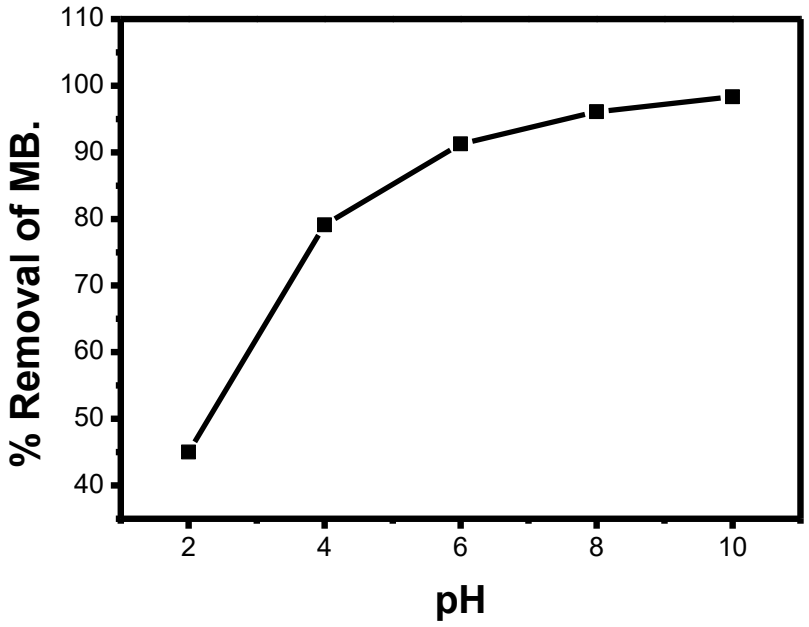

Fig. (8): Effect of pH on removal of (MB) on 25 wt. % Ag_2O/MCM-41.

Fig. 8 shows the role of pH on the removal of methylene blue dye by 25 wt. % Ag_2O/MCM-41. Evidently, a successive increase of adsorption of MB was observed with the increase of pH from 2.0-10.0. The removal of

ISSN: 0975-8585

methylene blue dye by nanoadsorbent is affected by the characteristic of the Ag_2O/MCM-41 surface and structure of dye molecular. Considering the effect of dye solution pH, one can assume adsorption of MB decreases at acidic pH is may be attributed to the existence of excess H^+ ions competing with the cation groups on the MB dye for adsorption active sites. The adsorption can also be described based on an electrostatic interaction among the ionic dye molecules and charged substance [28].

Effect of adsorbent dosage

The removal of (MB) and (BG) dyes by Ag_2O/MCM-41 nanoadsorbent were studied by changing the weight of adsorbent (0.01, 0.03, 0.05, 0.07 and 0.1g) with keeping pH value of 8.0, initial dyes concentration 100 mg/L, and 50 mL of adsorption solution for 240 min. The effect of adsorbent dosage on the removal of dyes is show in Fig. 9. The results reveal that the adsorption percentage removal increased from 58.39 to 92.97% for MB dye and the adsorption percentage removal increased from 55.64 to 88.56% for BG dye with increasing the nanoadsorbent weight from 0.05 g to 0.1g, respectively. The maximum adsorption efficiency was confirmed for MB and BG adsorption at 0.1g of adsorbent. It may be due to the large surface area of Ag_2O/MCM-41[29- 35].

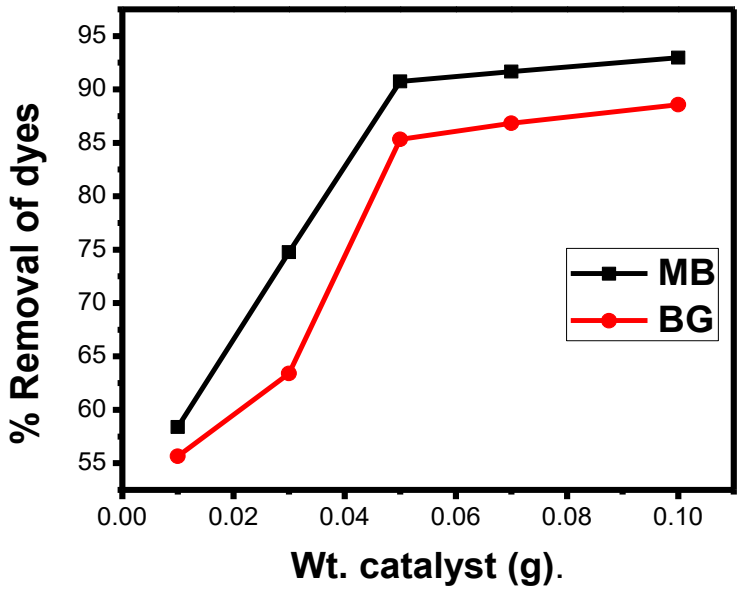

Fig. (9): Effect of the adsorbent dosage on removal of dyes on Ag_2O/MCM-41.

Effect of calcination temperature

The influence of calcination temperature of Ag_2O/MCM-41 on adsorption of MB and BG dyes (300, 400, 550 and 700°C) were investigated and displayed in Fig. 10. The results showed that the adsorption of MB and BG dyes for all samples at 550 °C was the best adsorption performance, and results showed that 25 wt. % Ag_2O/MCM-41 nanoadsorbent sample have the highest adsorption capacity. The decrease in the rate of removal of the dyes at calcination temperature 300 and 400ºC may be due to the presence of a small residual quantity of template on the surface of the catalyst. While the lower adsorption efficiency using adsorbent prepared at 700ºC is attributable to loss part of silver oxide at high calcination temperature.

ISSN: 0975-8585

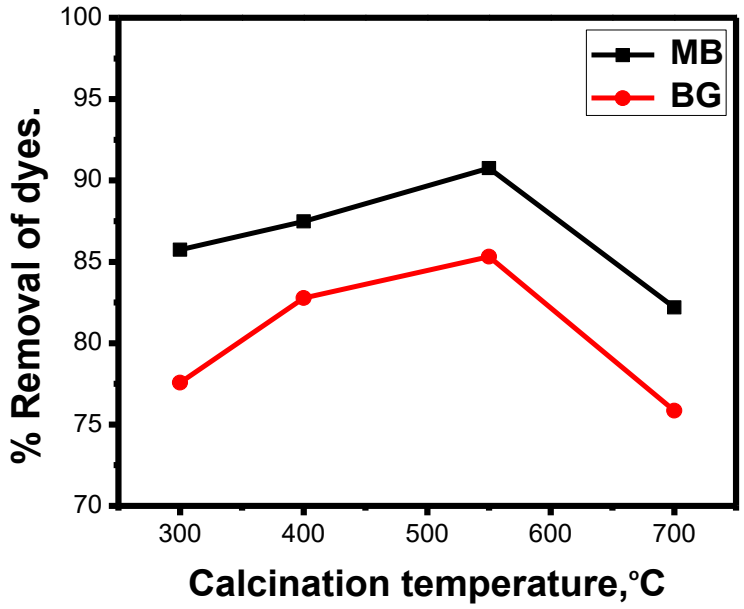

Fig (10): The % removal of dyes by 25 wt. % Ag_2O/MCM-41 at 300, 400, 550, and 700°C.

Effect of initial concentration

The effect of initial concentration of MB and BG dyes was studied in the range of 25- 300 mg/L at pH value of 8.0 and 50 mL of adsorption solution volume, and 0.05 g adsorbent for 240 min. Figure 11 shows the % removal of MB and BG dyes. From Fig.11, an increase in initial dye concentration is accompanied with observable decrease in adsorption capacity, which may be realated to the saturation of the available active site with the increase of the initial concentration of dyes [36-38].

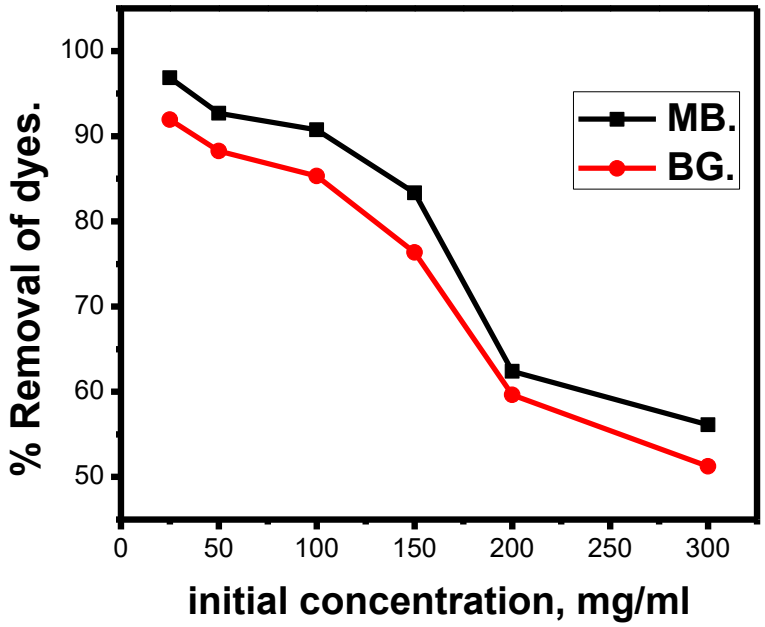

Fig (11): Effect of initial dyes conc. on removal of MB and BG dyes on 25 wt. % Ag_2O/MCM-41.

ISSN: 0975-8585

Langmuir adsorption isotherms

Linear adsorption models were fitted to calculate the adsorption parameters such as Langmuir and Freundlich equations (equation 1, 2, respectively) [38-43]

$$\frac{C_e}{q_e} = \frac{1}{K_L q_m} + \frac{C_e}{q_m} \quad (1)$$

Where q_e is the adsorption capacity (mg/g), q_{max} the maximum monolayer adsorption capacity of the adsorbent (mg/g), C_e the equilibrium dye concentration in the solution (mg/L), and K_L is Langmuir adsorption constant (L/mg) which is related to the heat of adsorption. Fig.13 shows the linear Langmuir plot. One of the important characteristics of the Langmuir isotherm can be exhibited by a dimensionless separation factor, R_L; which is defined as $R_L = \frac{1}{1+KC_0}$, Where C_o is maximum initial solute conc. and the R_L value indicates whether the adsorption is unfavorable ($R_L > 1$), linear ($R_L = 1$), favorable ($0 < R_L < 1$), or irreversible ($R_L = 0$). It was observed that the obtained R_L values in the range 0.0147 – 0.0386 for MB and BG, respectively indicating that the removal of MB and BG on Ag_2O/MCM-41 nanoadsorbents are favourable.

Freundlich adsorption isotherms

The following equation is the linearsed Freundlich plot form [33, 44]:

$$\log q_e = \frac{1}{n}\log C_e + \log K_F \quad (2)$$

Here, K_F and n are Freundlich constant related to removal rate and adsorption intensity, respectively. In general, $n > 1$ shows that adsorbate is favorably adsorbed on the adsorbent while $n < 1$ proves the adsorption process is chemical in nature.

The plot of ln (q_e) against ln (C_e) gave a straight line with a slope of 1/n and intercept of ln K_F. Figure 14 shows satisfactory linear plots indicating the fitting of MB and BG adsorption data to the Freundlich equation. The Freundlich constants determined from linear Freundlich plots, together with corresponding values of correlation coefficient values (R^2) are listed in the Table 1. The n values were found to be about 3.16 and 2.41 for MB and BG, respectively, which show that the adsorption is favourable and the process is physical in nature. Based on the obtained correlation coefficient values (R^2), it has been concluded that Langmuir model gives improved fitting result than Freundlich model Also the values of q_{max} and Langmuir constants determined by the application of the Langmuir model are included in the Table 1.

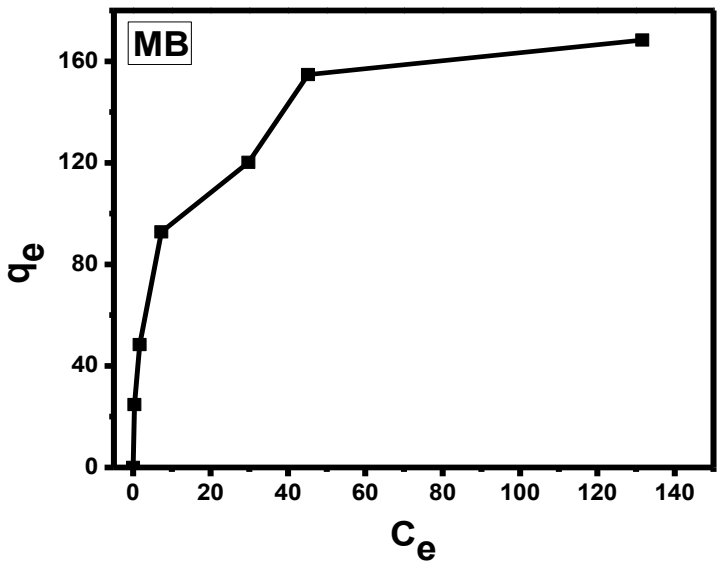

ISSN: 0975-8585

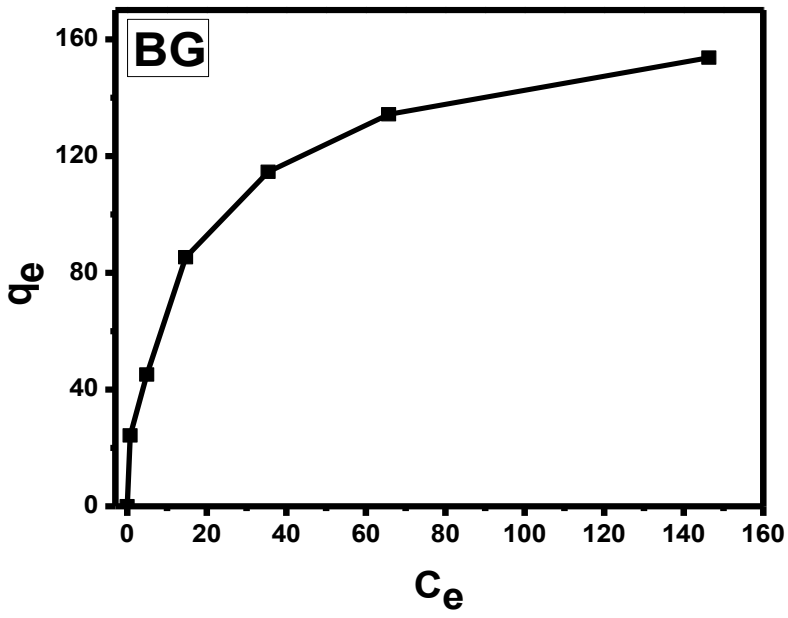

Fig. (12): Equilibrium adsorption isotherm of MB and BG dyes 25 wt. % Ag_2O/MCM-41.

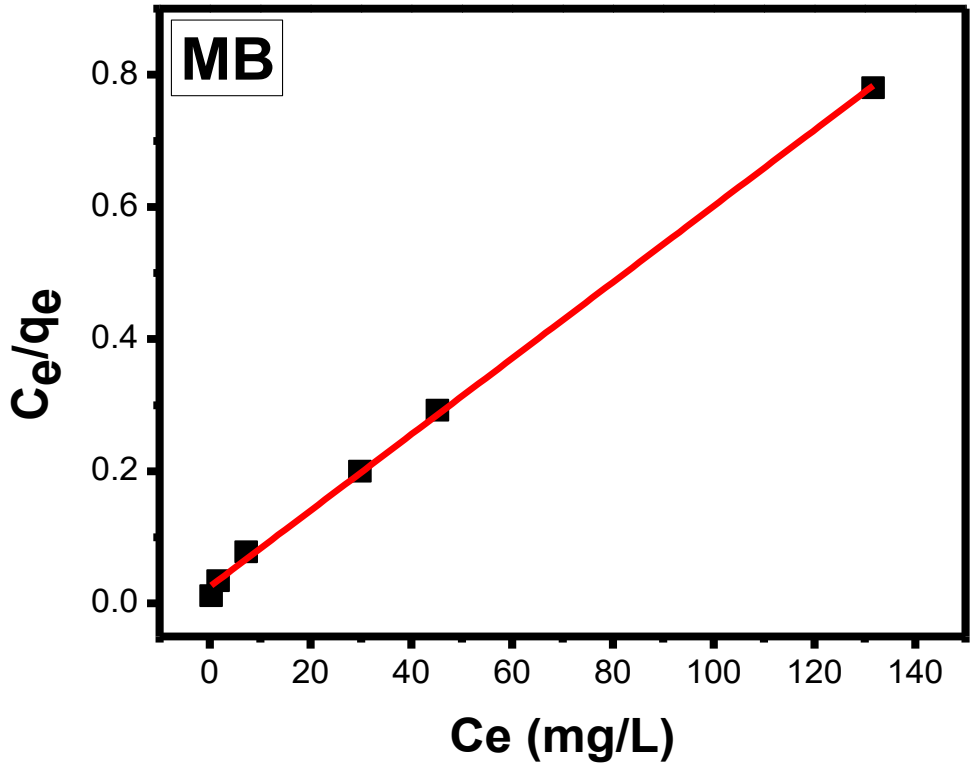

ISSN: 0975-8585

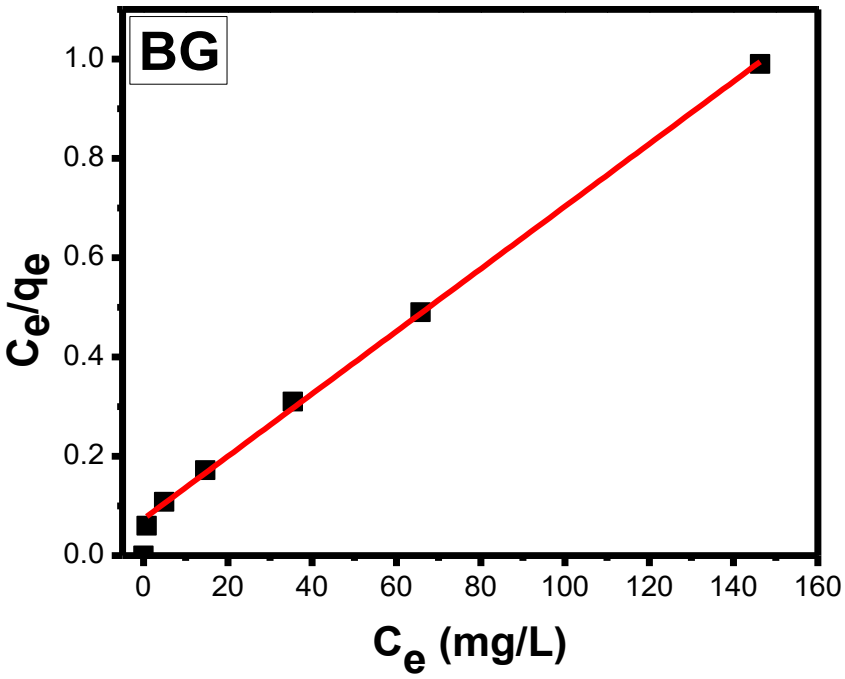

Fig. (13): a Linear form of Langmuir isotherm for (MB) and (BG) dyes onto 25 wt. % Ag_2O/MCM-41.

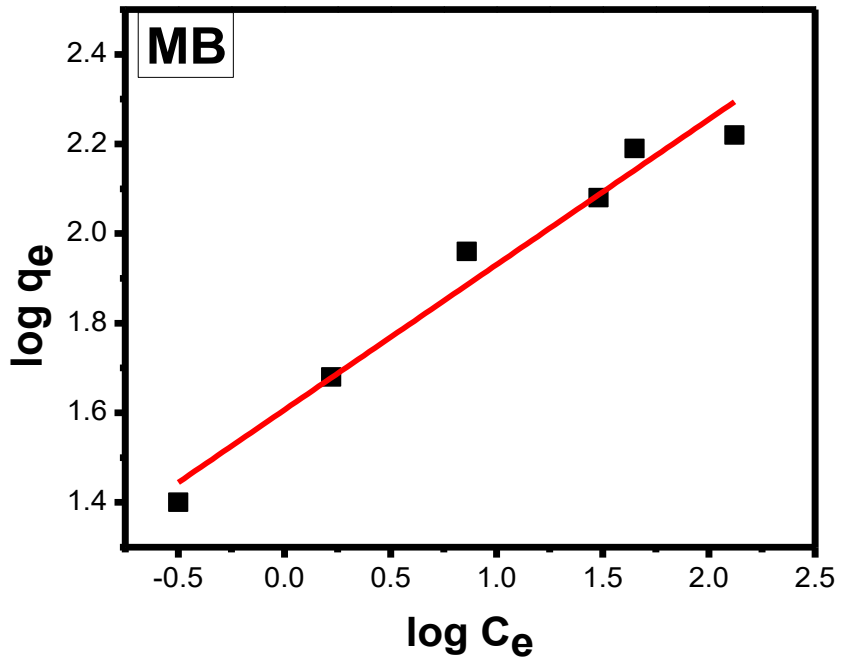

ISSN: 0975-8585

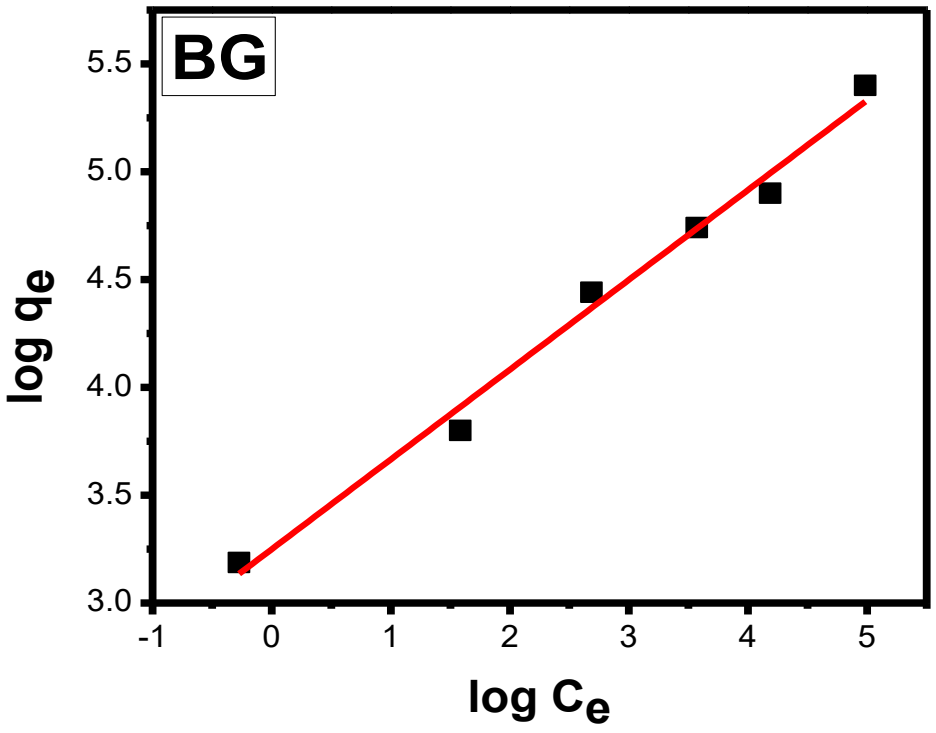

Fig. (14): a linear form of Freundlich isotherm for (MB) and (BG) dyes onto 25 % wt. Ag_2O/MCM-41.

Table (1): adsorption isotherm parameters for MB and BG dyes on 25 wt.% Ag_2O/MCM-41.

Sample	Langmuir isotherm				Freundlich isotherm		
	q_{max} (mg/g)	K_L (L/mg)	R^2	R_L	K_F (mg/g)	n	R^2
MB	175.4	0.223	0.9987	0.0147	4.96	3.16	0.94622
BG	161.3	0.083	0.9968	0.0386	25.25	2.41	0.97793

Effect of contact time

The adsorption of MB and BG dyes was studied at a different time intervals using 0.05 g of Ag_2O/MCM-41, pH value 8.0 and 100 mg/L of dyes solution. Fig. 15 and 16 show the effect of contact time from up to 240 minute on the adsorption efficiency of MB and BG dyes for all samples. The removal of MB and BG increases with time and reaches equilibrium after 30 min. The removal of MB and BG dyes on all samples of nanoadsorbent was quickly increased during the first 30 min, then gradual increase during 60 min and the adsorption process slowdown; this may be due to the great number of vacant sites available for adsorption at the initial adsorption period than the later stages.

The kinetic models used in order to study the mechanism of adsorption were the pseudo-first-order-kinetic and the pseudo-second-order-kinetic models.

Pseudo-first-order-kinetic model

The difference form of the pseudo-first-order model of adsorption can be described in the next equations [29- 32]:

ISSN: 0975-8585

$$\ln(q_e - q_t) = \ln q_e - k_1 t \quad (3)$$

Where q_e and q_t (mg/g) are the amounts of dyes adsorbed at equilibrium and at time t, respectively and $k_1$is the equilibrium concentration constant (min^{-1}).

Fig. 17 and 18 show the linear form of pseudo-first-order model to the kinetic adsorption for dyes. The kinetic parameters calculated on the basis of this model are presented in Table 2. The higher value of R^2 was equal to 0.96907 and 0.97754 for MB and BG adsorption kinetics respectively, and the predicted q_e values found from this kinetic model did not show good agreement with the experimental ones. This suggested that the removal of MB and BG by Ag_2O/MCM-41 nanoparticle dose not follow the pseudo-first-order kinetic model.

Pseudo-second-order-kinetic model

The differential form of the pseudo-second-order reaction equation may be written as [14, 45]:

$$\frac{t}{q_t} = \frac{1}{k_2 q_e^2} + \frac{1}{q_e} t \quad (4)$$

Where, K_2 is pseudo-second rate cons. ($mg.g^{-1}min^{-1}$).

Fig. 19 and 20 show the application of linear pseudo-second order model to the kinetic adsorption. Kinetic adsorption constants as determined by the application equations 4 are listed in the Table 3.

The results confirmed that the pseudo-second-order kinetic produced a good linearity. The high values of R^2 were found to be 0.99896 and 0.99991 for MB and BG adsorption and the experimental and calculated q_e values are very close. This suggested that the adsorption of dyes on Ag_2O/MCM-41 nanoparticle follow the pseudo-second-order kinetic model.

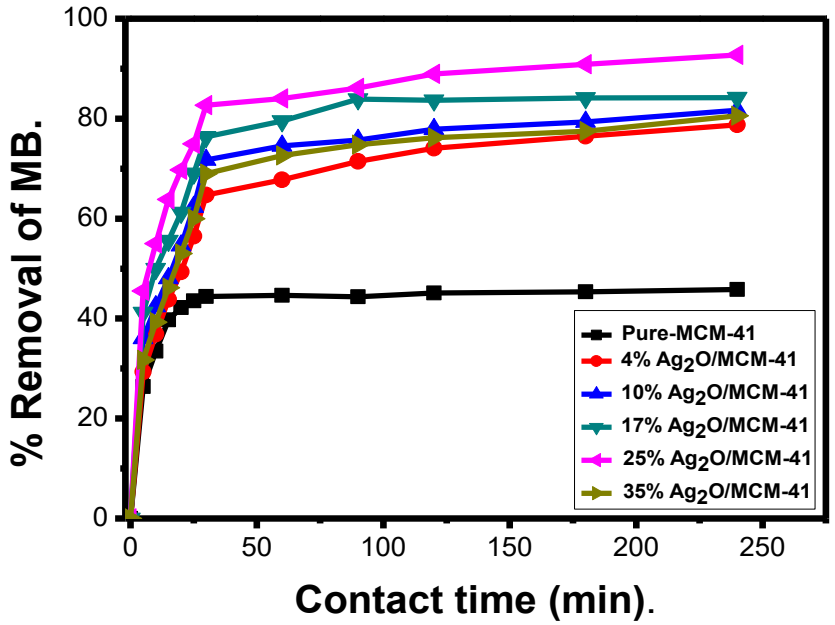

Fig. (15): Effect of contact time on removal of MB on 25 wt. % Ag_2O/MCM-41.

ISSN: 0975-8585

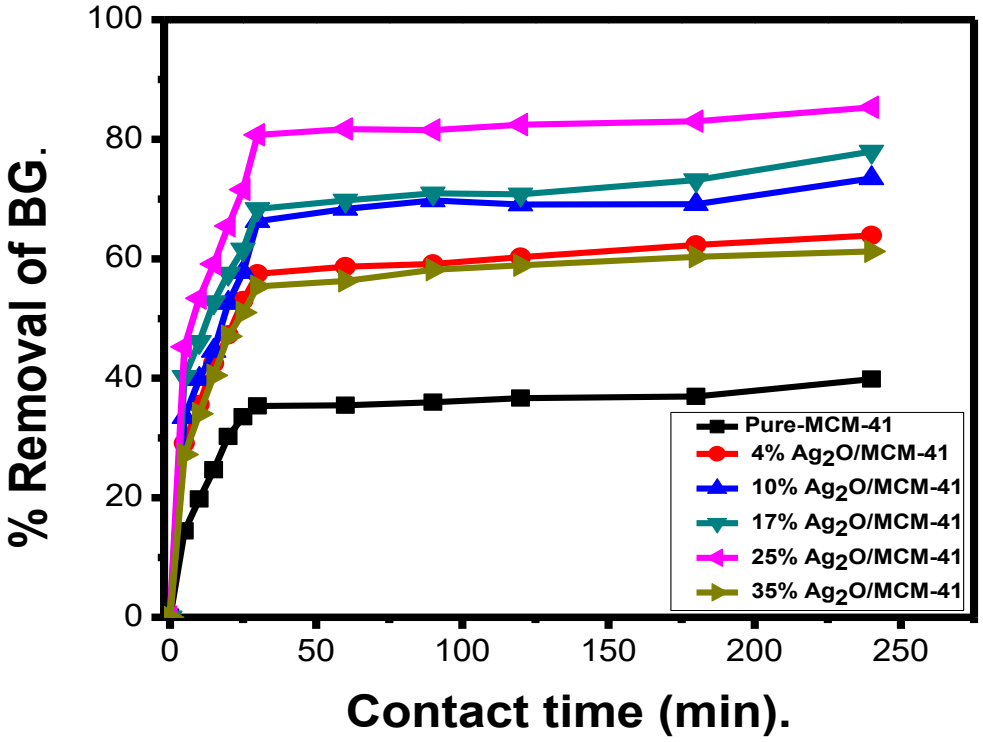

Fig. (16): Effect of contact time on removal of BG on 25 wt. % Ag_2O/MCM-41.

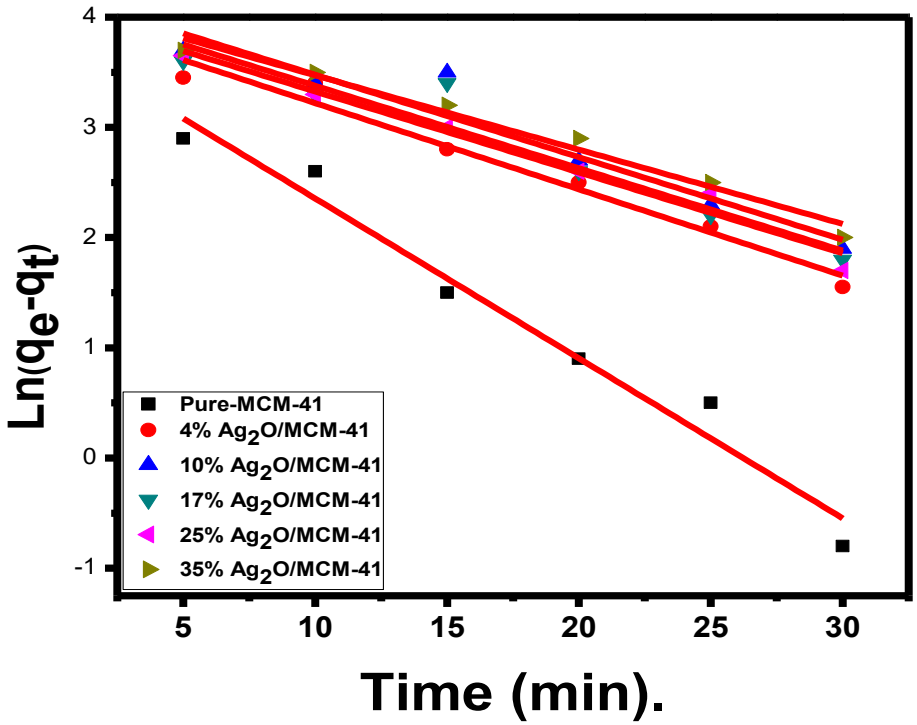

Fig. (17): Pseudo-first-order-kinetic model for adsorption of MB dye.

ISSN: 0975-8585

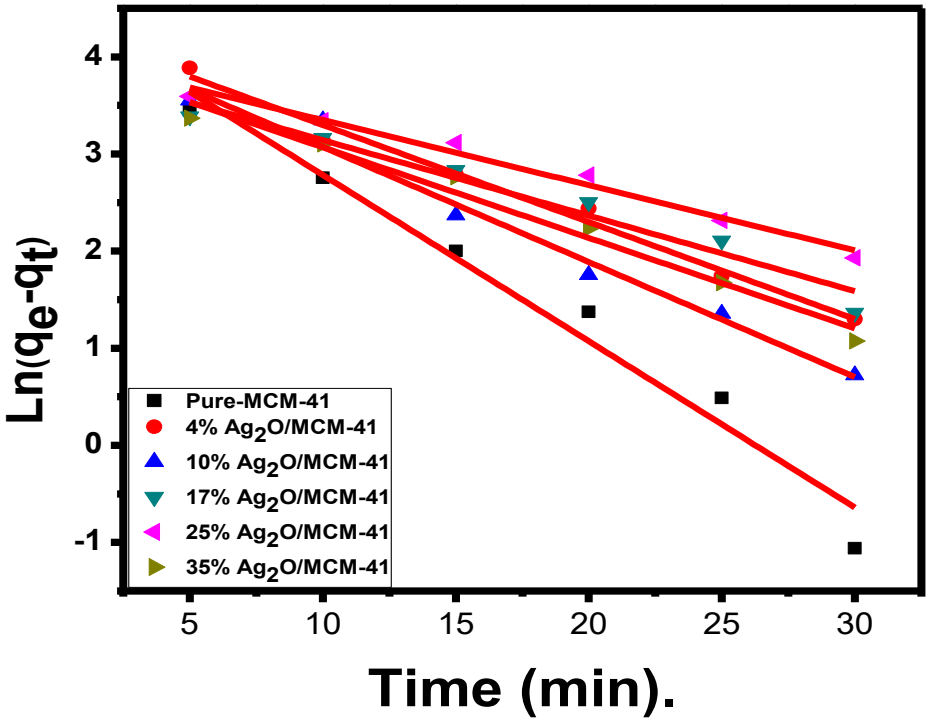

Fig. (18): Pseudo-first-order-kinetic model for adsorption of BG dye.

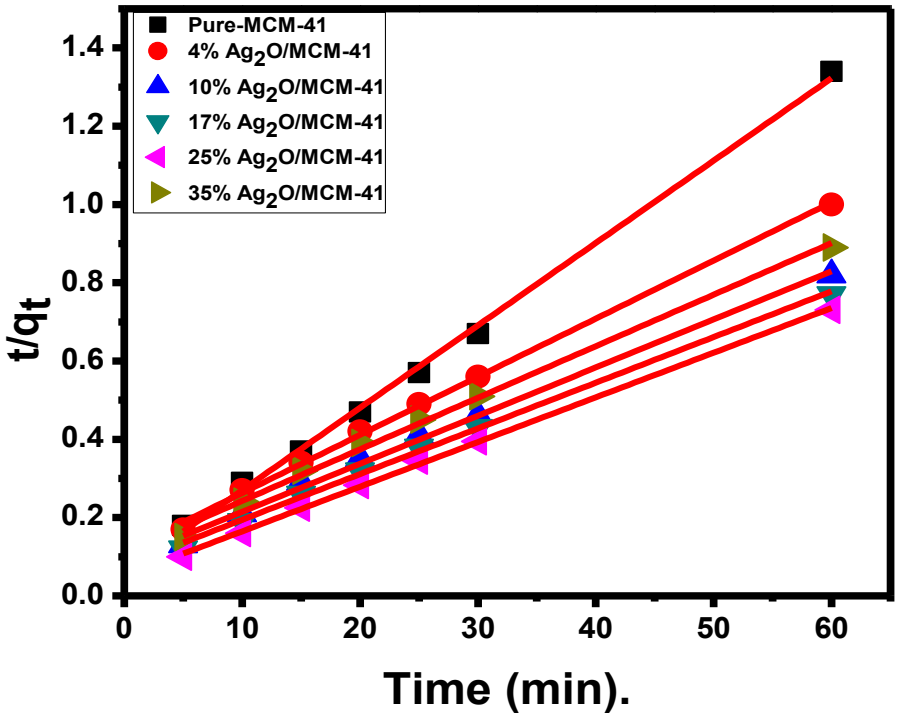

Fig. (19): Pseudo-second-order-kinetic model for adsorption of MB dye.

ISSN: 0975-8585

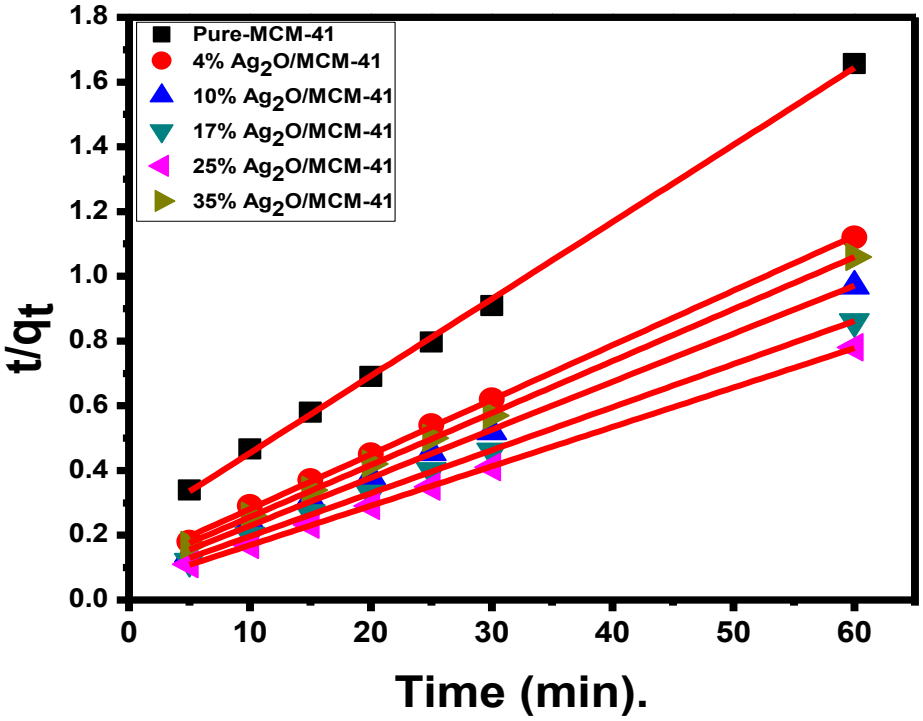

Fig. (20): Pseudo-second-order-kinetic model for adsorption of BG dye.

Table (2): kinetic model parameters (pseudo 1st order and pseudo 2nd order) for adsorption of methylene blue dye onto investigated adsorbent.

sample	$q_{e\ (Exp.)}$ (mg/g) after 1hr	Pseudo-first-order-kinetic model (MB)			Pseudo-second-order-kinetic model(MB)		
		q_{e1} (mg/g)	K_1 (1/hr.)	R^2	q_{e2} (mg/g)	K_2 (g/mg.hr)	R^2
MCM-41	44.67	45	0.334	0.96356	44.5	$8.49*10^{-3}$	0.9976
4% AgM	67.76	54.78	0.18	0.96508	67.34	$1.93*10^{-3}$	0.9985
10% AgM	74.56	68.48	0.172	0.90713	75.36	$1.92*10^{-3}$	0.9955
17% AgM	79.54	61.97	0.172	0.90713	80.68	$1.98*10^{-3}$	0.9974
25% AgM	84.05	57.97	0.169	0.96907	83.64	$2.81*10^{-3}$	0.9990
35% AgM	72.61	63.22	0.155	0.97283	72.87	$1.69*10^{-3}$	0.9953

Table (3): kinetic model parameters (pseudo 1st order and pseudo 2nd order) for adsorption of brilliant green dye onto investigated adsorbent.

sample	$q_{e\ (Exp.)}$ (mg/g) after 1hr	Pseudo-firs-order-kinetic model (BG)			Pseudo-second-order-kinetic model (BG)		
		q_{e1} (mg/g)	K_1 (1/hr)	R^2	q_{e2} (mg/g)	K_2 (g/mg.hr)	R^2
MCM-41	35.48	89.65	0.394	0.96349	35.01	$3.77*10^{-3}$	0.9989
4% AgM	58.68	73.47	0.230	0.98428	59.27	$2.53*10^{-3}$	0.9990
10% AgM	68.32	70.63	0.273	0.97541	67.34	$2.72*10^{-3}$	0.9988
17% AgM	69.78	50.42	0.179	0.94856	70.13	$3.20*10^{-3}$	0.9993
25% AgM	81.67	55.74	0.154	0.97754	82.16	$6.54*10^{-3}$	0.9999
35% AgM	56.31	54.6	0.214	0.97391	56.26	$3.30*10^{-3}$	0.9997

CONCLUSION

Ag_2O/MCM-41 nanoadsorbent with different ratios of Ag_2O were prepared by impregnation-evaporation method then calcined at 550 ºC for 2 h. XRD showed that Ag_2O/MCM-41 had uniform pore structure with hexagonal well- ordered arrangement. It was observed that the removal of dyes on Ag_2O/MCM-41 is increase by increasing weight ratio Ag_2O loaded to the samples. The best results were obtained with 25% Ag_2O/MCM-41 which shows higher adsorption activity. The adsorption was found to follow the pseudo-second-order adsorption kinetic model and fitted with Langmuir adsorption isotherm.

REFERENCES

[1] B. Boukoussa, R. Hamacha, A. Morsli, A. Bengueddach, Adsorption of yellow dye on calcined or uncalcined AL-MCM-41 mesopours materials, Arab.J.Chem, xxx (2013) xxx.

[2] L. De Rogatis, M. Cargnello, V. Gombac, B. Lorenzut, T. Montini, P. Fornasiero, Embedded phases: a way to active and stable catalysts, ChemSusChem 3 (2010) 24–42.

[3] H. Tüysüz, F. Schüth, Ordered mesoporous materials as catalysts, Adv. Catal. 55 (2012) 127–239.

[4] M. Vallet-Regí, F. Balas, D. Arcos, Mesoporous materials for drug delivery, Angew. Chem. Int. Ed. 46 (2007) 7548–7558.

[5] P. Yang, S. Gai, J. Lin, Functionalized mesoporous silica materials for con- trolled drug delivery, Chem. Soc. Rev. 41 (2012) 3679–3698.

[6] W.X. Mai, H. Meng, Mesoporous silica nanoparticles: a multifunctional nano therapeutic system, Integr. Biol. 5 (2013) 19–28.

[7] Sh. Sohrabnezhad, A. Sadeghi, Matrix effect of montmorillonite and MCM-41 matrices on the antibacterial activity of Ag2CO3 nanoparticles, Applied Clay Science 105–106 (2015) 217–224.

[8] Yuehong Shu, Yimin Shao, Xiangyu Wei, Xi Wang, Qiangqiang Sun, Qiuyun Zhang, Laisheng Li, Synthesis and characterization of Ni-MCM-41 for methyl blue adsorption, Microporous and Mesoporous Mater. 214 (2015) 88-94.

[9] S. Sarina, E. R. Waclawik and H. Zhu, Photocatalysis on supported gold and silver nanoparticles under ul- traviolet and visible light irradiation, Green Chemistry, (2013) 439-445.

[10] Dipti Prava Sahoo, Dharitri Rath, Binita Nanda and K. M. Parida, Transition metal/metal oxide modified MCM-41 for pollutant degradation and hydrogen energy production: a review, RSC Adv., 5 (2015) 83707

[11] Y. Zhu, J. Zhou, J. Hu, H. Liu, The effect of grafted amine group on the adsorption of CO2 in MCM-41: A molecular simlution, Catal. Today, 194 (2012)53.

[12] R. Kumar, M. A. Barakat, Decolourization of hazardous brilliant green from aqueous solution using binary oxidized cactus fruit peel, Chem. Eng. J, 226 (2013) 377.

[13] 5. E. Eren, O. Cubuk, H. Ciftcic, B. Eren, B. Caglar, Adsorption of basic dye from aqueous solutions by modified sepiolite: Equilibrium, kinetics and thermodynamics study, Desalination, 252 (2010) 88.

[14] M. P. Tavlieva, S. D. Genieva, V. G. Georgieva, L. T. Vlaev,Kinetic study of brilliant green adsorption from aqueous solution onto white rice husk ash, J. Colloid and Interface Sci., 409 (2013) 112.

[15] M. A. M. Salleh, D. Kh. Mahmoud, W. A. W. Abdul Karim, A. Idris,Cationic and anionic dye adsorption by agricultural solid wastes: A comprehensive review, Desalination, 280 (2011) 1.

[16] X. Yang, Q. Guan, W. Li,Effect of template in MCM-41 on the adsorption of aniline from aqueous solution,J. l. Environ. Management, 92 (2011) 2939.

[17] M. A. Khraisheh, M. A. Al-Ghouti, S. J. Allen, M. N. Ahmed,Effect of OH and silanol groups in the removal of dyes from aqueous solution using diatomite, Water Res., 39 (2005) 922.

[18] A. A. Ibrahim, S. E. Samra, H. A. Mostafa, Preparation characterization of some solid acid mesoporous, Mansoura niversity, 2012.

[19] M. Zhao, Z. Tang, P. Liu, M. Zhao, Removal of methylene blue from aqueous solution with silica nano-sheets derived from vermiculite, J. Hazard. Mater, 158 (2008) 43.

[20] J. Li, M. Cui, Z. Cuo, Z. Liu and Z. Zhu, Preparation of p–n junction BiVO4/Ag2O heterogeneous nanostructures with enhanced visible-light photocatalytic activity, Mater. Latt., 151 (2015) 75.

[21] R. Huanga, B. Lana, Z. Chenb, H. Yana, Q. Zhanga, j. binga, L. Li, Catalytic ozonation of p-chlorobenzoic acid over MCM-41 and Fe loaded MCM-41, Chem. Eng. J., 180 (2012) 19– 24

[22] R. Olivrira, F. Camilo and M. Bizeto, Evaluation of the influence of sulfur-based functional groups on the embedding of silver nanoparticles into the pores of MCM-41, J. S. S. Chem. 235 (2016) 125.

[23] A. S. Al-Hobaib, K. M. AL-Sheetan, M. R. Shaik, N. M. Al-Andis and M. S. Al-Suhybani, of Reverse Osmosis Membranes Modified with Ag2O Nanoparticles to Improve Performance, Nano. Rese. Lette. 10 (2015) 379.

[24] L. F. Chen, L. E. Norena, j. Navarrete, J. A. Wang, Improvement of surface acidity and structural regularity of Zr-modified mesoporous MCM-41, Mater Chem. Phys., 97 (2006) 236.

[25] D. Chena, Z. Qu, Y. Lv, X. Lu, W. Chena, X. Gao, Effect of oxygen pretreatment on the surface catalytic oxidation of HCHO on Ag/MCM-41 catalysts, J. Molec. Cata. A: Chem., 404-405 (2015) 98.

[26] D. Chen, Z. Q, W. Zhang, X. Li, Q. Zhao, Y. Shi, TPD and TPSR studies of formaldehyde adsorption and surface reaction activity over Ag/MCM-41 catalysts, Colloids and Surfaces A: Phys. Eng. Aspects 379 (2011) 136.

[27] P. Das, S. Ray, A. Bhaumik, B. Banerjee, and C. Mukhopadhyay, Cubic Ag2Onanoparticle incorporated mesoporous silica with large bottle-neck like mesopores for the aerobic oxidative synthesis of disulfide, RSC Adv., 5 (2015) 6323.

[28] X. Xiao, F. Zhang, Z. Feng, S. Deng and Y. Wang, Adsorptive removal and kinetics of methylene blue from aqueous solution using NiO/MCM-41 composite, Phys. E 65 (2015) 4.

[29] D. M. Marzouqa, M. B. Zughul, M. O. Taha, H. A. Hodali,Effect of particle morphology and pore size on the release kinetics of ephedrine from mesoporous MCM-41 materials, J. Porous Mater., 19 (2012) 825.

[30] K. Dimos, P. Stathi, M. A. Karakassides, Y. Deligiannakis, Synthesis and characterization of hybrid MCM-41 materials for heavy metal adsorption, Microporous and Mesoporous Mater., 126 (2009) 65.

[31] X. Sheng, J. Gao, L. Han, Y. Jia, W. Sheng,One-pot synthesis of tryptophols with mesoporous MCM-41 silica catalyst functionalized with sulfonic acid groups, Microporous and Mesoporous Mater., 143 (2011) 73.

[32] S. Eftekhari, A. Habibi-Yangjeh and S. Sohrabnezhad, Application of AlMCM-41 for competitive adsorption of methylene blue and rhodamine B: Thermodynamic and kinetic studies. J. Hazard. Mater., 178 (2010) 349.

[33] H. Chaudhuri, S. Dash and A. Sarkar, Adsorption of different dyes from aqueous solution using Si-MCM-41 having very high surface area, J. Por. Mater., 23 (2016) 1227.

[34] Weirui Chen, Xukai Li, Zhaoqi Pan, Yixiang Bao, Sushuang Ma, Laisheng Li, Efficient adsorption of Norfloxacin by Fe-MCM-41 molecular sieves: Kinetic, isotherm and thermodynamic studies, Chemi. Eng. J., 281 (2015) 397.

[35] M. saif Ur Rehma. M. Munir, M. A. Shfaq, N. Rashid, M. F. Nazar, M. Danisd, J. I. Han, Adsorption of brilliant greean dye from aqueous solution onto red caly, Chem. Eng. J, 228 (2013) 54

[36] Y. Shu, Y. Shao, X. Wei, X. Wang, Q. Sun, Q. Zhang and L. Li, Synthesis and characterization of Ni-MCM-41 for methyl blue adsorption, Microporous Mesoporous Mater., 214 (2015) 88.

[37] A. M. B. Furtado, Yu Wang, T. G. Glover, M. D. LeVan, MCM-41 impregnated with active metal sites: Synthesis, characterization, and ammonia adsorption, Microporous and Mesoporous Mater. 142 (2011) 730.

[38] C. Lee, S. Liu, L. Juang, C. Wang,K. Lin, M. Lyu, Application of MCM-41 for dyes removal from wastewater, J. o Haza. Mater. 147 (2007) 997.

[39] J. Feng, S. Y. Song, Y. Xing, H. J. Zhang, Z. F. Li, L. N. Sun, X. M. Guo, W.Q. Fan, Synthesis, characterization, and near-infrared luminescent properties of the ternary thulium complex covalently bonded to mesoporous MCM-41,J. Solid State Chem., 182 (2009) 435.

[40] K. G. Bhattacharyya, A. Sarma, Adsorption characteristics of the dye, Brilliant Green, on Neem leaf powder, Dyes and Pigments, 57 (2003) 21.

[41] C. Weng, Y. Pan, Adsorption of a cationic dye (methylene blue) onto spent activated clay, J. Hazard. Mater.,144 (2007) 355.

[42] M. A. Zanjanchi, H. Golmojdeh, M. Arvand, Enhanced adsorptive and photocatalytic achievements in removal of methylene blue by incorporating tungstophosphoric acid-TiO_2 into MCM-41, J. Hazard. Mater., 169 (2009) 233.

[43] S. K. Theydana, M. J. Ahmed, Adsorption of methylene blue onto biomass-based activated carbon by $FeCl_3$ activation: Equilibrium, kinetics, and thermodynamic studies, J. Analy. App. Pyro., 97 (2012) 116.

[44] I. Langmuir, The constitution and fundamental properties of solids and liquids, J. Am. Chem. Soc., 40 (1918) 1361.

[45] H. Freundlich, Die adsorption inlusungen, J. Phys. Chem., 57 (1906) 385.